

A LINEAR ACOUSTIC MODEL FOR INTAKE WAVE DYNAMICS  
IN I.C. ENGINES

**M.F. Harrison<sup>\*1</sup> and P.T. Stanev<sup>1</sup>**

\* corresponding author

Professional addresses:

<sup>1</sup> School of Engineering, Cranfield University,  
Cranfield, Bedfordshire MK43 0AL, England

Correspondence to:

Dr Matthew Harrison  
School of Engineering  
Whittle Building  
Cranfield University  
Cranfield  
Bedfordshire MK43 0AL

**ABSTRACT**

In this paper, a linear acoustic model is described that has proven useful in obtaining a better understanding of the nature of acoustic wave dynamics in the intake system of an internal combustion (IC) engine. The model described has been developed alongside a set of measurements made on a Ricardo E6 single cylinder research engine.

The simplified linear acoustic model reported here produces a calculation of the pressure time-history in the port of an IC engine that agrees fairly well with measured data obtained on the engine fitted with a simple intake system.

The model has proved useful in identifying the role of pipe resonance in the intake process and has led to the development of a simple hypothesis to explain the structure of the intake pressure time history: the early stages of the intake process are governed by the instantaneous values of the piston velocity and the open area under the valve. Thereafter resonant wave action dominates the process. The depth of the early depression caused by the moving piston governs the intensity of the wave action that follows. A pressure ratio across the valve that is favourable to inflow is maintained and maximised when the open period of the valve is such to allow at least, but no more than, one complete oscillation of the pressure at its resonant frequency to occur whilst the valve is open.

## 1 Introduction

In this paper, a linear acoustic model is described that has proven useful in obtaining a better understanding of the nature of acoustic wave dynamics in the intake system of an internal combustion (IC) engine.

Excellent engine performance requires the simultaneous combination of good combustion and good engine breathing. Whilst good combustion depends only in part on the characteristics of the flow within the combustion chamber, good engine breathing is strongly affected by the unsteady flow in the intake manifold, and to a lesser extent, that in the exhaust manifold.

There has been much research on calculating the effects of unsteady flow in intake and exhaust manifolds. Reference [1] provides a good summary of the history of the topic over the last several decades. History tells us that correctly harnessing the unsteady flow in the intake manifold of a naturally aspirated I.C. engine can yield improvements in engine torque of 10% or more, whereas performing the equivalent in the exhaust manifold yields a more modest 3-5%.

Previous studies of unsteady flows in I.C. engine manifolds have mostly used one-dimensional gas-dynamic theory. Reference [2] is a well-known text where the Method of Characteristics is used to solve the one dimensional, non-linear, gas-dynamic equations in space and time. Reference [3] is a more recent alternative. When the amplitude of the unsteady component of pressure in a manifold is sufficiently low, the propagation of such a disturbance is well described by linear

acoustic theory [4]. Under such conditions, the tuning of manifold geometry to improve engine performance becomes an exercise in applied acoustics. There is recent evidence to support the use of linear acoustic theory at sound pressure levels in excess of 165 dB [5].

The work presented here is restricted to the intake system only. Although the unsteady flow in the exhaust manifold is of interest to engine developers and exhaust silencer manufacturers alike, the high sound intensity levels in the pipes suggests the use a non-linear gas-dynamic approach rather than an acoustic such as this one. When carefully interrogated, the results of non-linear gas-dynamic calculations can reveal secrets of the unsteady exhaust flow that cannot be readily measured. For example, reference [6] shows a calculation of the unsteady flow velocity through an exhaust valve.

The linear acoustic model developed in this work offers an alternative to non-linear gas-dynamic calculations and has proved realistic for the unsteady flow in the intake manifold of a naturally aspirated I.C. engine. Because it views the problem of intake flow as one of applied acoustics, it is hoped that the model promotes a different perspective on what is otherwise a well-studied system. The authors are not claiming that this method is particularly unique, but it does have the useful attribute of being very simple and yet proving realistic in practice

The complex nature of intake flows has made their understanding a difficult task, hence the long history of research on the problem. The complexity arises for several reasons:

- (i) The intake flow is unsteady. The flow velocity over the back of the intake valves may reach 300+ m/s for short periods of the intake stroke but once the valve closes it is strictly zero.
- (ii) The flow through the valve is coupled to the wave dynamics in the port. High rates of unsteady flow cause intense wave action. When sufficiently intense these waves can influence the unsteady flow. Hence, the unsteady flow is both a cause and a result of wave action.
- (iii) When sufficiently intense, the wave action may exhibit non-linear behaviour.
- (iv) There are many points in an intake system where wave energy may be reflected. A complex sound field results from the sum of many reflections.
- (v) For the case of multi-cylinder engines, waves caused in separate ports may propagate and interfere with one another.
- (vi) The flow may cause secondary sources of flow noise. Such flow noise is particularly excited by the expansion chambers [7] and orifices [8] commonly found in intake systems. The understanding of the flow noise problem is under continuous development.

The first five complexities may be accommodated within a non-linear, time marching iterative model of the wave action. Such models calculate time histories for the unsteady pressure velocity, density and temperature in the intake system. Together,

these describe the intake process and their scrutiny is therefore worthwhile. However, the causes of these fluctuations remain mysterious, concealed in the iterative numerics required for their calculation.

A simpler model is sought to explain the causes of fluctuating pressure and velocity in the intake port. The model presented here makes the following assumptions with respect to the six complexities described above:

- (i) Only two flow states are considered. When the intake valve is open a single time-average flow velocity is calculated for that open period. When the valve is closed, the net flow velocity is taken to be zero.
- (ii) A simplified model of the intake process is obtained where the unsteady flow through the valve and the wave action in the port are un-coupled. The unsteady flow causes the wave action but the wave action is not allowed to influence the unsteady flow.
- (iii) Linear, plane wave acoustic theory is used to calculate the wave action thus neglecting any non-linear effects.
- (iv) A simple straight pipe intake system is used to minimise the number of locations at which sound is reflected.
- (v) A single cylinder engine is considered in order to remove interactions in the waves caused by different cylinders.

- (vi) The influence of flow induced noise is neglected.

## **2 The test case**

The model described here has been developed alongside a set of measurements made on a Ricardo E6 single cylinder research engine. The 0.5 litre engine was fitted with a rather long intake pipe (1.4 m) and a fixed venturi carburettor 400mm from the intake valve, as shown in Figure 1. A large airbox fitted with an orifice plate was used to measure air consumption rates. A previous study had confirmed that the pressure of the airbox had negligible effect on the wave action in the intake pipe [9]. Kistler Type 4045A2 pressure sensors were fitted in the intake port and elsewhere in the intake pipe. A slotted disk fitted to the end of the crankshaft and an optical sensor gave an indication of instantaneous crankshaft position. The engine was run and also motored at various speeds in the range 1000-2000 rev/min<sup>-1</sup> and the signals from the pressure and optical sensors were digitised using an Iotech Daqbook200 system.

## **3 The physics of the intake process**

Figure 2 shows a sketch of the intake process. During the intake stroke, an annulus of turbulent flow develops over the back of the opening valve and is eliminated when the valve shuts once more. The magnitude and direction of the flow is dictated by the ratio of unsteady pressures either side of the valve. A favourable pressure ratio for inflow to the cylinder occurs when the pressure in the cylinder is lower than the pressure in the port. Such a favourable pressure ratio may be obtained in two ways: firstly, by the rapid downward motion of the piston reducing the cylinder pressure and

secondly, by the wave action in the port increasing the instantaneous pressure in the port.

Evidence of these two mechanisms may be found in measured traces of the fluctuating pressure in the port. Figure 3 shows the port pressure for one engine cycle, both with the engine run and motored at around  $1900 \text{ rev/min}^{-1}$ . Note that the speeds shown in Figure: 3 and subsequent figures are slightly different in both cases. The speeds quoted are those calculated for the particular cycle for which data is displayed. When firing, the engine speed varies from cycle to cycle, whereas the variation is minimal when the engine is motored. Figure 3 is worthy of some further discussion.

Firstly, for the firing engine the opening of the intake valve (IVO) is shortly followed by a prolonged pressure depression once the exhaust valve is closed. The full depth of this depression occurs when the crankshaft has turned  $90^\circ$  after top dead centre (90 ATDC), which corresponds to the peak piston velocity. The pressure rises quickly after the depression producing a pressure peak sometime between bottom dead centre (BDC) and the closing of the intake valve (IVC). The prevailing static pressure is a little below 1.0 bar. It is noteworthy that the depth of the depression relative to the static pressure is equal to the height of the pressure peak relative to the same datum.

The hypothesis for explaining the shape of the pressure trace is this: until the depression reaches its greatest depth, the pressure time history is governed by the effects of the downwards accelerating piston and the opening valve, thereafter it is governed by wave action. The height of the pressure peak depends on the depth of



the depression that proceeds it and that in turn is determined by the maximum piston velocity and the flow area of the opening valve. The realism and the generality of this hypothesis will be explored throughout this paper.

In addition, Figure 3 shows that the firing of the engine has little effect on the wave action in the intake port. The only significant difference results from small pressure peak in the valve overlap period (IVO-EVC) for the motored case. Here, poor scavenging of the cool air results in high exhaust back pressure late in the exhaust stroke and the valve overlap causes reversed flow of air into the intake port and a temporary pressure peak therein.

A spectrum of the motored pressure is also shown in Figure 3. This spectrum has been obtained by digitising long sequences of pressure data at a sample frequency of 4096 Hz and by using a moving Hanning window to produce an average of one hundred 2048 point FFTs with a spectral resolution of 2 Hz. The pressure oscillation in Figure: 3 is occurring at 64Hz at 1877 rev/min, when the valve opens 15.6 times every second. The wave action is, therefore, occurring as a 4<sup>th</sup> harmonic of the valve actuating frequency. By measuring the crankshaft rotation delay between pressure peaks it is clear that the oscillation is occurring at around 64Hz when the valve is open as well as closed.

The generality of the points raised by the inspection of Figure 3 is investigated by inspecting the results obtained at other running speeds. Figure 4 shows the intake port pressure at around 1700 rev/min<sup>-1</sup> and Figure 5 shows data at around 1500 rev/min<sup>-1</sup>. The points raised for Figure 3 generally apply to Figure 4 except in the latter case the

pressure fluctuation is occurring at 56Hz rather than 64Hz. However, 56Hz remains a 4<sup>th</sup> harmonic of the valve actuation frequency at 1690 rev/min<sup>-1</sup>.

The data in Figure 5 shows some important differences to that of Figure 3. Firstly, the pressure fluctuates at 64Hz once more but this time it is the 5<sup>th</sup> harmonic of the valve actuation frequency at 1523 rev/min. In addition, because the fluctuation frequency is the same but the engine speed is lower, whereas in Figure 3 the pressure was above the 1 bar of atmospheric pressure at IVC, in Figure 5 the pressure has had time to dip below 1 bar by IVC.

The fact that 64Hz appears as the dominant frequency at two different engine speeds suggests resonant behaviour in the intake pipe.

It seems that the intake pipe has a resonance at a frequency around 60Hz, both when the valve is open and when it is closed, this being the average of 56Hz and 64Hz. When it is closed, the resonant frequencies of the open/closed pipe are given by:

$$f = \frac{nc}{4x} \quad (1)$$

which for  $n = 1, 3, 5 \dots$ ,  $c = 343\text{m/s}$ ,  $x = 1.4\text{m}$  then  $f_{n=1} = 61.25\text{Hz}$  and the agreement is good.

Resonance at frequencies corresponding to odd numbers of quarter wavelengths are to be expected in this case where the intake pipe has a noise source (the unsteady flow through the intake valve) at one end and an open un-flanged termination at the other end. Consider Figure: 6 where the right hand end of the figure corresponds to the open

end of the intake pipe. This end may be viewed as a pressure-release surface where the two travelling waves in the pipe must be in anti-phase at the open end. This anti-phase produces a pressure minimum at the open end accompanied by a particle velocity maximum.

Resonance in the pipe will be found when a high sound level is radiated from the open end of the pipe when the excitation at the source is only small. This occurs when the pipe is odd integers of a quarter wavelength long.

Our earlier hypothesis of the nature of the intake process can now be extended, thus:

The early stages of the intake process are governed by the instantaneous values of the piston velocity and the open area under the valve. Thereafter resonant wave action dominates the process. The depth of the early depression caused by the moving piston governs the intensity of the wave action that follows. A pressure ratio across the valve that is favourable to inflow (i.e. one where the pressure in the port is higher than the pressure in the cylinder) is maintained and maximised when the open period of the valve is such to allow at least, but no more than, one complete oscillation of the pressure at its resonant frequency to occur whilst the valve is open. Much less, or much more than one complete oscillation will result in a lower pressure in the port during the final closing moments of the valve and hence diminished inlet flow.

The implications of this hypothesis are as follows. Firstly, the wave action will intensify as mean piston speeds increase, thus, as engine speeds increases. Secondly, there will be a narrow range of speeds at which the benefits of a strong and favourable pressure ratio will be enjoyed. At lower speeds, more than one depression will reduce

the benefit. At higher speeds the maximum possible pressure ratio will not be reached before IVC.

## **4 Description of the model**

The model used in this paper will be described in four sections. Firstly, an equivalent acoustic circuit will be presented. Secondly, a model for the unsteady flow through the valve will be described along with some sample output. Thirdly, a model for the resonant wave action in the intake pipe will be described, again with sample output. Finally, the integration of the components into a single model will be discussed. Results for the final model will be shown in Section 5.

### **4.1 Overview of the model**

The model may be described using the equivalent acoustic circuit shown in Figure 7. Acoustic circuits have been used elsewhere to describe either the intake or the exhaust process in IC engines and in compressors [10-16] but these usually show a constant pressure source with a series impedance.

Referring to Figure 7, the intake process is described here as two acoustic loads  $Z_e$  and  $Z_1$  acting on a volume velocity source of strength  $V_s$  and producing an acoustic pressure  $P_1$  immediately at the port side of the valve seat. This seems more realistic than the use of a constant pressure source. Relating this to the sketch of the intake process shown in Figure 2,  $Z_1$  is the specific acoustic load impedance of the intake port and pipe applied to an acoustic source of strength  $V_s$  and specific source

impedance  $Z_e$ , these two together characterising the unsteady flow through the valve.

Note the continuity of pressure with:

$$P_1 = Z_e U_e = Z_1 U_1 \quad (2)$$

and the discontinuity in volume velocity with:

$$U_e = U_s - U_1 = \frac{P_1}{Z_e} \quad (3)$$

Now, the wave action in the intake port is described by the pair  $P_1$  and  $U_1$ . These may be calculated with a knowledge of  $U_s$ ,  $U_e$  and  $Z_1$ .

If the source impedance is very high, or indeed non-existent as an entity that is separable from  $Z_1$ , then  $U_e = 0$  and:

$$U_s = \frac{P_1}{Z_1} \quad (4)$$

The observation that the resonant frequency in the intake pipe is the same when the valve is open as when the valve is closed suggests that the source impedance is always high and under the parallel impedance model of Figure 7 its effects will be negligible and, hence, it may be neglected. Thus, the intake problem is reduced to the solution of equation 4.

## 4.2 A sub-model for the acoustic source strength $U_s$

In Section 4.1 the assumption  $U_s = U_1$  was put forward for a given intake pipe of cross-sectional area  $S_1$ , we can write:

$$U_s = u_1 S_1 \quad (5)$$

Where  $U_s$  is the volume velocity ( $\text{m}^3/\text{s}$ ) strength of the source, which in turn is the volume velocity through the intake valve and  $u_1$  is the acoustic particle velocity in the intake port.  $U_s$  is time varying and it is a function of the rate of change of cylinder volume  $V_d$  and of the instantaneous flow area under the valve  $S_v$  [17]. A simple, yet dimensionally correct relationship would be:

$$U_s = \frac{dV_d}{dt} \times \frac{S_v}{S_1} \quad (6)$$

Figure 8 shows the rate of change of cylinder volume calculated for the Ricardo E6 engine with a bore of 76.6mm, a stroke of 110mm and a compression ratio of 10.0 running at 1891 rev/min. Figure 9 shows the changing area under the opening intake valve, as measured on the test engine fitted with a single intake valve of 35mm diameter and a maximum lift of 9.5mm. The limiting area seen in the data is that of the 35mm diameter intake port. Applying the data from Figures 8 and 9 to Equation 6 yields a calculation of  $U_s$  shown in Figure 10. Small reverse flows are shown shortly after IVO and shortly before IVC. These are due to the timings of IVO and IVC being  $8^\circ$  BTDC and  $33^\circ$  ABDC respectively.

Figure 10 is reproduced as Figure 11 along with the spectrum of  $U_s$ . The single cycle shown in Figure 10 was repeated many times in a long sequence and by using a moving Hanning window to produce an average of one hundred 1024 point FFTs the spectrum shown in Figure: 11 was produced with a spectral resolution of around 1Hz due to the sample frequency being 1008Hz. It is clear that every integer harmonic of the valve actuation frequency of 15.75Hz is present in this spectrum. The 63Hz component is close to the value of 61.25Hz calculated as the lowest resonance of the intake pipe and this explains the dominance of the 64Hz component found in the intake pressure at this speed (Figure 3).

Figure 12 shows the same analysis for a speed of 1690 rev/min. The 56Hz component of  $U_s$  is responsible for the dominant 56Hz component of the intake pressure noted in Figure 4.

Figures 13 and 5 show the same effect at 64Hz, this time for a speed of 1523 rev/min.

### **4.3 A sub-model for the load impedance $Z_1$**

A one dimensional, linear, plane wave, frequency domain model of the intake pipe has been prepared following the well-established method developed by Davies [18].

The reference point for the model is the acoustic reflection coefficient  $r$  for an unflanged pipe [19]. At plane  $x = 0$  this gives the ratio of the amplitude of positive and negative going wave components  $p_o^+$  and  $p_o^-$  respectively, thus:

$$r_o = \frac{p_o^-}{p_o^+} \quad (7)$$

An end correction of length  $l$  accounts for the phasing of  $p_o^+$  and  $p_o^-$ , thus:

$$r = R_e^{i\theta} = -R_e^{i2kl} \quad \text{where } k \text{ is the wavenumber} \quad (8)$$

Values for  $R$  and  $l$  vary with the mean Mach number of the inlet flow [20].

The wave components at the intake valve can be transformed along the pipe length  $x$ , thus:

$$p_1^+ = p_o^+ e^{ik^*(x+l)} \quad (9)$$

$$p_1^- = p_o^- e^{-ik^*(x+l)} \quad (10)$$

Where  $k^*$  is a complex wavenumber taking Mach number and visco-thermal attenuation effects into consideration [18]. The specific load impedance ratio is given

by:

$$\zeta_1 = \frac{1+r_1}{1-r_1} \quad (11)$$

and

$$Z_1 = \zeta_1 \rho_o c_o S_1 \quad c_o = \text{stagnation sound speed} \quad (12)$$

$$\rho_o = \text{stagnation speed density}$$



Two spectra of  $Z_1$  need calculation, one for the open valve case and one for the closed valve case. For the closed valve case, the mean inlet Mach number is found from:

$$M = \frac{\int_{IVO}^{IVC} U_s dt}{S_1 c_o} \quad (13)$$

The mean inlet Mach number for the open valve is higher than this by the factor  $720 / (IVC-IVO)$ .

The outputs of the  $Z_1$  model are shown in Figure 14 for the speed of 1891 rev/min. The presence of higher mean flow for the open valve case shifts resonant frequencies downwards slightly compared with the closed valve case. Also the magnitude of the specific impedance ratio is altered. Note that resonances occur at values of  $n = 1, 3, 5, 7$  times the lowest natural frequency of 63Hz as anticipated by equation (1).

For the calculations, a slightly reduced pipe length of 1.31mm was used to account for the presence of a carburettor and other flow discontinuities not shown in Figure 1. This revised length was found by experiment using a wave decomposition technique [21] to directly measure the specific acoustic impedance spectrum and then by altering the pipe length in the theoretical model until the theory matched experiment.

#### 4.4 A sub-model for the port pressure $P_1$

Following on from equations 4 and 12:

$$P(t) = \text{IFFT}[U_s(f) \times Z_1(f)] \quad (14)$$

$U_s(f)$  is found by taking a single 64 point FFT of the 64 points used in the model to describe  $U_s$  for one cycle. The result of this is shown in Figure 15. The apparent coarse spectral resolution is a result of the limited temporal resolution of  $U_1$  being only 64 points to describe the  $221^\circ$  of crankshaft rotation between IVO and IVC.

In order to obtain the product in equation 14, the specific acoustic impedance ratio spectrum shown in Figure 14 should be recalculated to be a 64 point double sided spectrum with a resolution that matches  $U_s(f)$ . Such a spectrum is shown in Figure: 16.

The inverse Fourier transform of equation 14 must be performed twice, once for the open valve values of  $Z_1$  and once for the closed valve values. The resulting time histories of  $P_1$  are shown for 1891 rev/min in Figure 17.

In order to complete the calculation of  $P_1$ , the 64-point sequences from equation 14 must first be interpolated to 720-point sequences, one value for each degree of crankshaft rotation in the four-stroke cycle. The first few data points from the open valve sequence correspond to the values of  $P_1$  for the interval IVO-IVC. The

corresponding values from the closed valve sequence are discarded. The remaining values from the closed valve sequence correspond to the values of  $P_1$  for the period when the valve is closed. The pressure in the intake system will be the composite  $P_1$  added to the prevailing static pressure.

## 5 Results and Discussion

The model described in Section 4 has been used to calculate  $P_1$  in the intake port of the Ricardo E6 engine at three speeds: 1877, 1661 and 1523 rev/min. These are shown along with measured port pressures in Figures 18, 19 and 20 respectively. The validation of the calculations is good. There are obvious discontinuities in the calculated results at IVO and at IVC as the calculated pressure record is a composite of the results from two separate calculations.

The spectrum of the sound pressure level in the intake port is found by taking the FFT of one cycle of measured and calculated data at each speed and the results are shown in Figures 21, 22 and 23. The agreement between measured and calculated results is good at the lowest resonant frequency of the intake pipe but is prone to error at higher frequencies.

There are three possible causes for the differences between the measured and calculated results. The first may be that the model is over-simplified, and in particular the linear plane wave assumption may be inappropriate or the effects of flow-induced noise neglected in the model may be significant in practice. Some researchers report non-linear behaviour in intake ports [22] but there is no evidence of this here. The

second may be lack of realism in the model for  $Z_1$ , although such models have validated well in the past [11]. The third and most likely cause of differences is the model employed for  $U_s$  which neglects the source impedance and is decoupled from the acoustic load  $Z_1$ . The sensitivity of the validation to the output from the  $U_s$  model has been investigated using a second decoupled model for  $U_s$ .

Figure 24 shows the output from the  $U_s$  model described in Section 4.2. In addition the results from a second model are shown where the open flow area under the valve (Figure 9) is appropriately scaled to yield a second estimate of  $U_s$ . The scaling factor is calculated such that the two estimates of  $U_s$  agree at the start of the velocity profile and at only one other subsequent point. No physical significance is placed on this choice of scaling, it is merely convenient and appears to be effective. This second model for  $U_s$  has been used to produce Figures 25-30 that can be compared directly with Figures 18-23.

The results obtained using the second model for  $U_s$  are a little better than those obtained using the first model but differences between measured and calculated results remain.

In order to better quantify these differences, the  $P_1$  data for one cycle from Figures 25, 26 and 27 respectively have been repeated many times to form long data sequences. By using a moving Hanning window to produce averages of one hundred 4096 point FFTs the spectra shown in Figures: 31, 32, 33 were produced with a spectral resolution of 2-3Hz due to the sample frequency being between 9 - 11 kHz across the three speeds.

It is clear that the model used to calculate  $P_1$  is reliable at the lowest resonant frequency of the intake pipe but tends to underestimate the spectral content at harmonics of the valve actuation frequency that are not coincident with that lowest resonant frequency. For that reason, the calculated traces for  $P_1$  look like smooth modulations of a single resonant frequency, whereas the measured results are invariably more jagged in shape.

It is interesting to note that changing the shape of the  $U_s$  time history did not radically affect the calculated values of  $P_1$ . This suggests that finding a third uncoupled model for  $U_s$  is unlikely to improve the realism of the calculations and that the need to couple the acoustic source with its load is inevitable if improvements on the current method are to be made.

## **6 Conclusions**

The simplified linear acoustic model reported here produces a calculation of the pressure time-history in the port of an IC engine that agrees fairly well with measured data obtained on a single cylinder research engine fitted with a simple intake system.

The model has proved useful in identifying the role of pipe resonance in the intake process and has led to the development of a simple hypothesis to explain the structure of the intake pressure time history. That hypothesis is:

The early stages of the intake process are governed by the instantaneous values of the piston velocity and the open area under the valve. Thereafter resonant wave action

dominates the process. The depth of the early depression caused by the moving piston governs the intensity of the wave action that follows. A pressure ratio across the valve that is favourable to inflow is maintained and maximised when the open period of the valve is such to allow at least, but no more than, one complete oscillation of the pressure at its resonant frequency to occur whilst the valve is open.

Future improvements to the method will have to concentrate on the coupling between the unsteady flow through the valve (the acoustic source) and the wave action in the intake pipe (the acoustic load).

### **Acknowledgements**

The authors gratefully acknowledge the support of EPSRC under Grant No: GR/R04324 for this work.

## References

- 1 D E Winterbone, R J Pearson, 1999  
*Design Techniques for Engine Manifolds – Wave Action Methods for IC Engines*  
Professional Engineering Publishing
- 2 R. S. Benson, 1982  
*The thermodynamics and gas dynamics of internal combustion engines – Volume 1*  
Clarendon Press, Oxford
- 3 M. Borel, 2000  
*Les phenomenes d’ondes dans les moteurs*  
Editions Technip, Paris
- 4 A Onorati, 1994, Journal of Sound and Vibration, 171(3), pp369-395  
*Prediction of the acoustical performances of muffling pipe systems by the method of characteristics*
- 5 K.R. Holland, P.O.A.L. Davies, D.C. van der Walt, Journal of the Acoustical Society of America, 2002, 112 (5), Pt1, (in press)  
*Sound power flux measurements in strongly excited ducts with flow*

- 6 Y. Sathyanarayana, M.L. Munjal, 2000, *Applied Acoustics*, 60, pp425-450  
*A hybrid approach for aeroacoustic analysis of the engine exhaust system.*
- 7 P.O.A.L. Davies, K.R. Holland, 2001, *Journal of Sound and Vibration*, 239(4),  
695-708  
*The observed aeroacoustic behaviour of some flow-excited expansion chambers*
- 8 P. Durrieu, G. Hofmans, G. Ajello, R. Boot, Y. Auregan, A. Hirschberg,  
M.C.A.M. Peters, *Journal of the Acoustical Society of America*, 2001, 110(4),  
1859-1872  
*Quasisteady aero-acoustic response of orifices*
- 9 Sotiris Gritsis, 2001  
*Internal Combustion Engine Intake Acoustics*  
MSc Thesis, Cranfield University
- 10 P.O.A.L. Davies, 1996, *Journal of Sound and Vibration*, 190(3), 345-362,  
*Aerocoustics and time varying systems*
- 11 P.O.A.L. Davies & M.F. Harrison, 1997, *Journal of Sound and Vibration*,  
202(2), 249-274, *Predictive acoustic modelling applied to the control of intake/exhaust noise of internal combustion engines*



- 12 H. Boden & F Albertson, 2000, Journal of Sound and Vibration, 237(1), 45-65, *Linearity tests for in-duct acoustic one-port sources*
- 13 W.M. Wang, 1967, Journal of the Acoustical Society of America, Vol. 41, No. 6, p1418-1423, *Matrix formulation in acoustical analysis of mechanically driven fluid systems*
- 14 W.M. Wang, 1967, Journal of the Acoustical Society of America, Vol. 42, No. 6, p1244-1249, *Acoustical analysis of a multi-cylinder engine air-induction system*
- 15 L. Desmons & J. Kergomard, 1994, Applied Acoustics, Vol. 41, p127-155, *Simple analysis of exhaust noise produced by a four cylinder engine*
- 16 K.S. Peat & J.G. Ih, 2001, Journal of Sound and Vibration, 244(5), p821-835, *An investigation of the indirect measurement method of estimating the acoustic impedance of a time varying source.*
- 17 T.W. Asmus, 1982, SAE Paper No. 820749, *Valve events and engine operation*
- 18 P O A L Davies, 1988, Journal of Sound and Vibration, 124(1), pp91-115  
*Practical Flow Duct Acoustics*

- 19 P O A L Davies, J L Bento Coelho, M Bhattacharya, 1980, Journal of Sound and Vibration, 72(4), pp543-546  
*Reflection coefficients for an unflanged pipe with flow*
- 20 P O A L Davies, 1987, Journal of Sound and Vibration, 115(3), pp560-564  
*Plane wave reflection at flow intakes*
- 21 P. O. A. L. Davies, J. L. Bento Coelho, M. Bhattacharya, 1980, J. Sound Vib. 72(4), 539-542, Measurement of plane wave acoustic fields in flow ducts.
- 22 J S Lamancusa, K B Todd, 1989, Transactions of ASME, Journal of Vibration, Acoustics, Stress and Reliability in Design, Vol 111, 199-207  
*An experimental study of induction noise in four-cylinder internal combustion engines*

## Figure captions

- Figure: 1 Single cylinder test engine
- Figure: 2 Sketch of the intake process
- Figure: 3 Average spectrum of a long motored pressure time history.  
Motored  $1891 \text{ revmin}^{-1}$ (solid line), firing  $1877 \text{ revmin}^{-1}$ (dashed line).
- Figure: 4 Average spectrum of a long motored pressure time history  
Motored  $1690 \text{ revmin}^{-1}$ (solid line), firing  $1661 \text{ revmin}^{-1}$ (dashed line).
- Figure: 5 Average spectrum of a long motored pressure time history  
Motored  $1523 \text{ revmin}^{-1}$ (solid line), firing  $1523 \text{ revmin}^{-1}$ (dashed line).
- Figure: 6 Sketch of resonance in the intake pipe
- Figure: 7 Acoustic model
- Figure: 8 Rate of change of cylinder volume.  $-1891 \text{ revmin}^{-1}$ .
- Figure: 9 Instantaneous flow area under the open intake valve
- Figure: 10 Calculated volume velocity through the intake valve  
 $-1891 \text{ revmin}^{-1}$ .
- Figure: 11 Calculated volume velocity through the intake valve with spectrum  
 $-1891 \text{ revmin}^{-1}$ .
- Figure: 12 Calculated volume velocity through the intake valve with spectrum  
 $-1690 \text{ revmin}^{-1}$ .
- Figure: 13 Calculated volume velocity through the intake valve with spectrum  
 $-1523 \text{ revmin}^{-1}$ .
- Figure: 14 Calculated acoustic load impedance  
Open valve  $1891 \text{ revmin}^{-1}$ (solid line), closed valve  $1891 \text{ revmin}^{-1}$ (dashed line).
- Figure: 15 FFT of calculated volume velocity  $-1891 \text{ revmin}^{-1}$ .
- Figure: 16 Double sided spectrum of calculated acoustic load  $Z_1$ .  
 $-1891 \text{ revmin}^{-1}$ .

- Figure: 17      Calculated records for  $P_1$ .  
Open valve 1891  $\text{revmin}^{-1}$ (solid line), closed valve 1891  $\text{revmin}^{-1}$ (dashed line).
- Figure: 18      Calculated and measure intake port pressures.  
Measured 1877  $\text{revmin}^{-1}$ (solid line), calculated 1877  $\text{revmin}^{-1}$ (dashed line).
- Figure: 19      Calculated and measure intake port pressures.  
Measured 1661  $\text{revmin}^{-1}$ (solid line), calculated 1661  $\text{revmin}^{-1}$ (dashed line).
- Figure: 20      Calculated and measure intake port pressures.  
Measured 1523  $\text{revmin}^{-1}$ (solid line), calculated 1523  $\text{revmin}^{-1}$ (dashed line).
- Figure: 21      Calculated and measure intake port pressure spectra.  
Measured 1877  $\text{revmin}^{-1}$ (solid line), calculated 1877  $\text{revmin}^{-1}$ (dashed line).
- Figure: 22      Calculated and measure intake port pressure spectra.  
Measured 1661  $\text{revmin}^{-1}$ (solid line), calculated 1661  $\text{revmin}^{-1}$ (dashed line).
- Figure: 23      Calculated and measure intake port pressure spectra.  
Measured 1523  $\text{revmin}^{-1}$ (solid line), calculated 1523  $\text{revmin}^{-1}$ (dashed line).
- Figure: 24      Alternative ways of calculating  $U_1$ .  
Based on changing cylinder volume 1891  $\text{revmin}^{-1}$  (solid line), based on scaled valve area 1891  $\text{revmin}^{-1}$ (dashed line).
- Figure: 25      Calculated and measure intake port pressures, using the second model for  $U_1$ .  
Measured 1877  $\text{revmin}^{-1}$ (solid line), calculated 1877  $\text{revmin}^{-1}$ (dashed line).
- Figure: 26      Calculated and measure intake port pressures, using the second model for  $U_1$ .  
Measured 1661  $\text{revmin}^{-1}$ (solid line), calculated 1661  $\text{revmin}^{-1}$ (dashed line).
- Figure: 27      Calculated and measure intake port pressures, using the second model for  $U_1$ .  
Measured 1523  $\text{revmin}^{-1}$ (solid line), calculated 1523  $\text{revmin}^{-1}$ (dashed line).

- Figure: 28      Calculated and measure intake port pressure spectra, using the second model for  $U_1$ .  
Measured 1877  $\text{revmin}^{-1}$ (solid line), calculated 1877  $\text{revmin}^{-1}$ (dashed line).
- Figure: 29      Calculated and measure intake port pressure spectra, using the second model for  $U_1$ .  
Measured 1661  $\text{revmin}^{-1}$ (solid line), calculated 1661  $\text{revmin}^{-1}$ (dashed line).
- Figure: 30      Calculated and measure intake port pressure spectra, using the second model for  $U_1$ .  
Measured 1523  $\text{revmin}^{-1}$ (solid line), calculated 1523  $\text{revmin}^{-1}$ (dashed line).
- Figure: 31      Calculated and measure intake port pressure spectra, using the second model for  $U_1$ .  
Measured 1877  $\text{revmin}^{-1}$ (solid line), calculated 1877  $\text{revmin}^{-1}$ (dashed line).
- Figure: 32      Calculated and measure intake port pressure spectra, using the second model for  $U_1$ .  
Measured 1661  $\text{revmin}^{-1}$ (solid line), calculated 1661  $\text{revmin}^{-1}$ (dashed line).
- Figure: 33      Calculated and measure intake port pressure spectra, using the second model for  $U_1$ .  
Measured 1523  $\text{revmin}^{-1}$ (solid line), calculated 1523  $\text{revmin}^{-1}$ (dashed line).

Figures

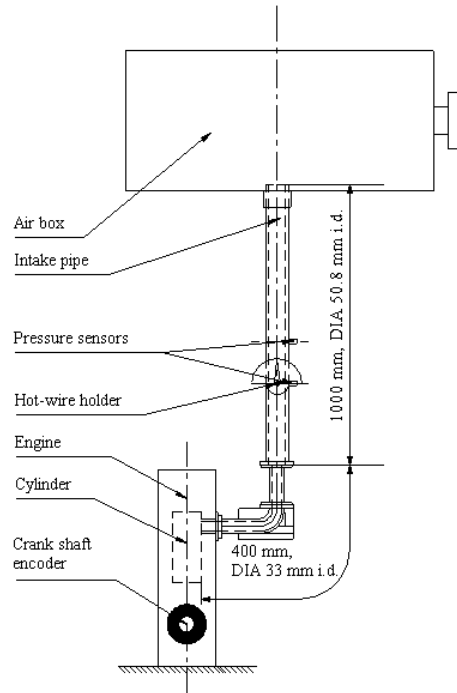
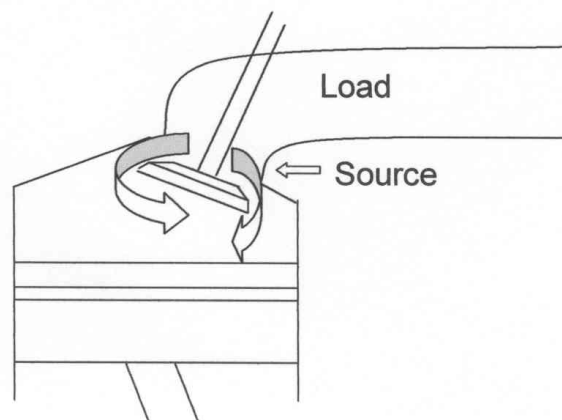


Figure: 1

Figure: 2



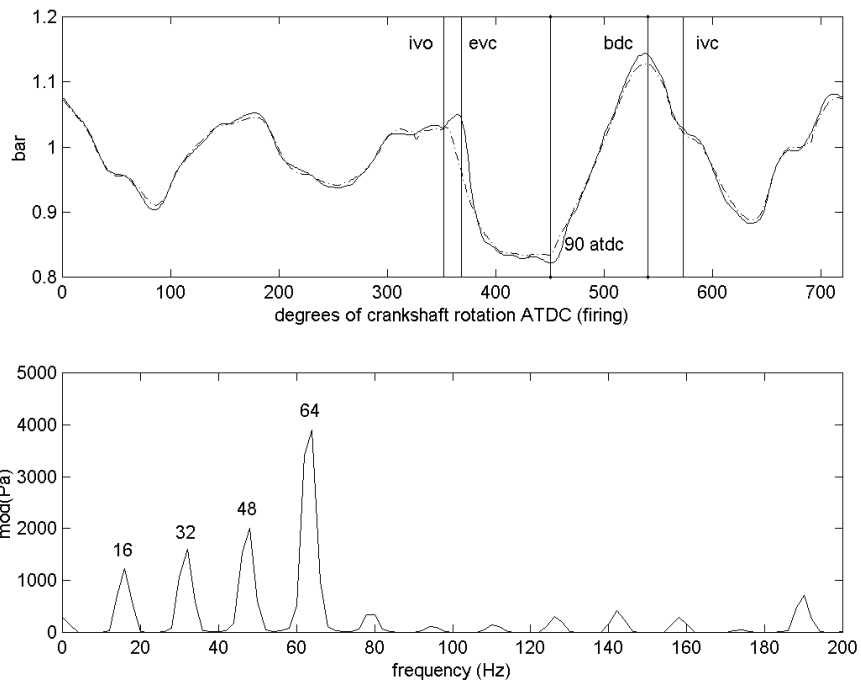


Figure: 3

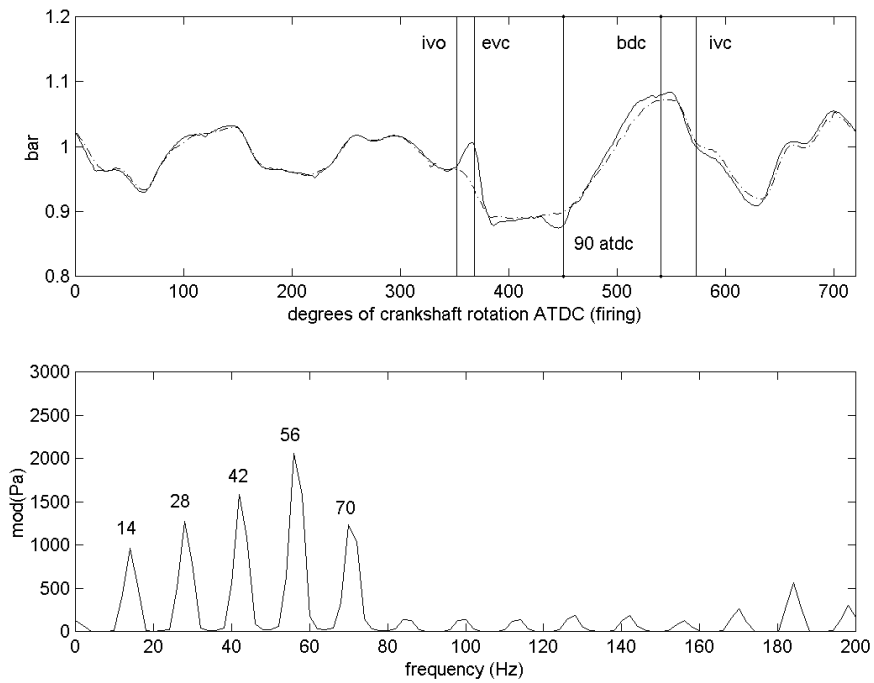


Figure: 4

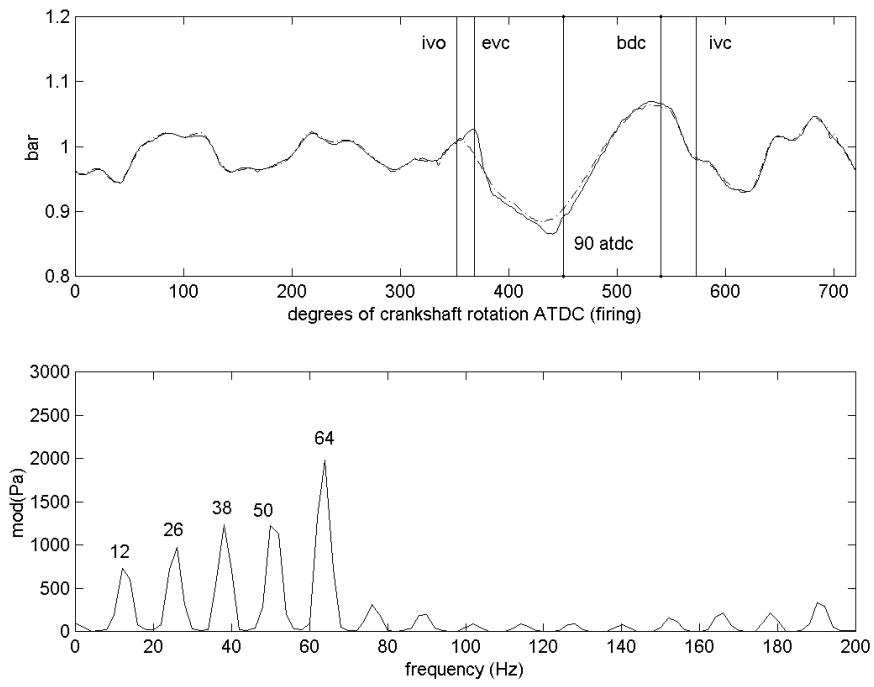


Figure: 5

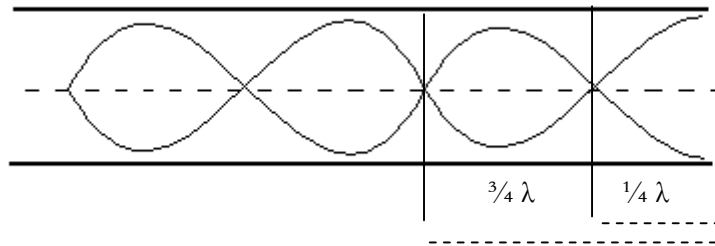


Figure: 6



Figure: 7

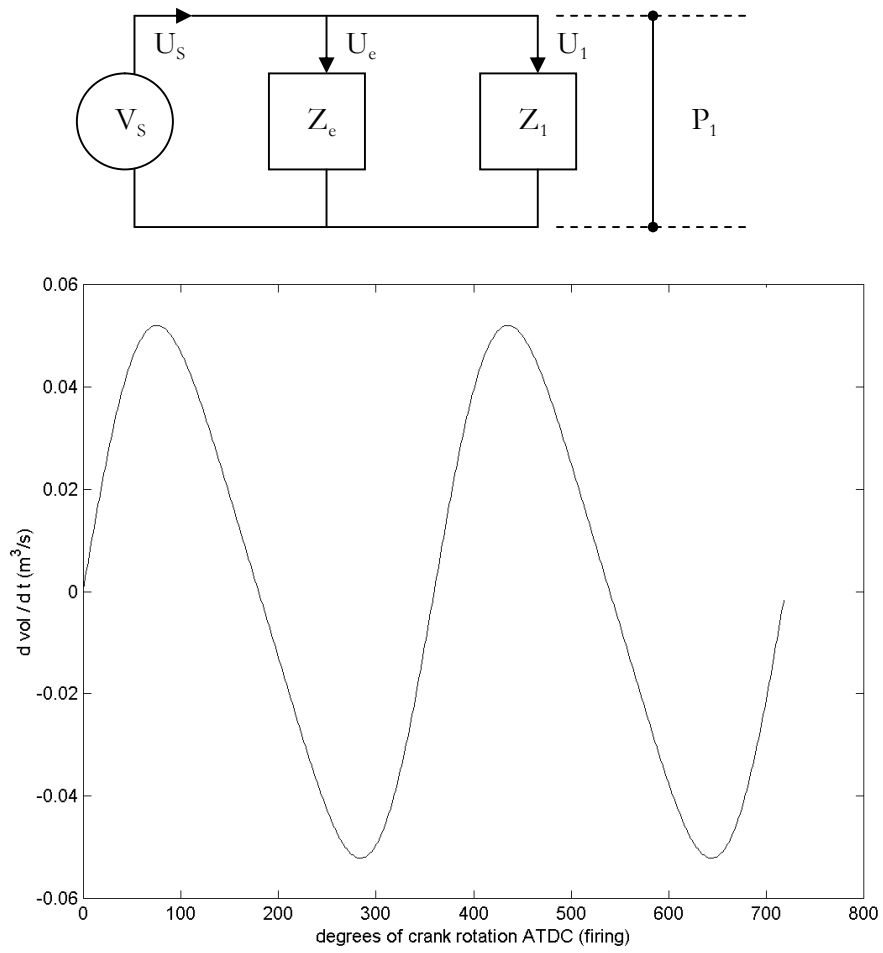


Figure: 8

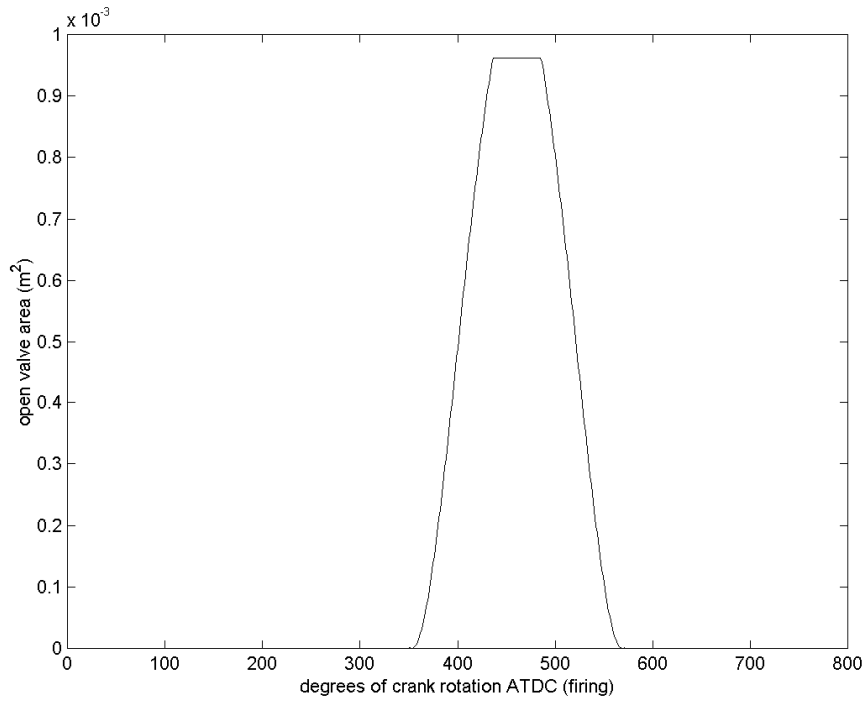


Figure: 9

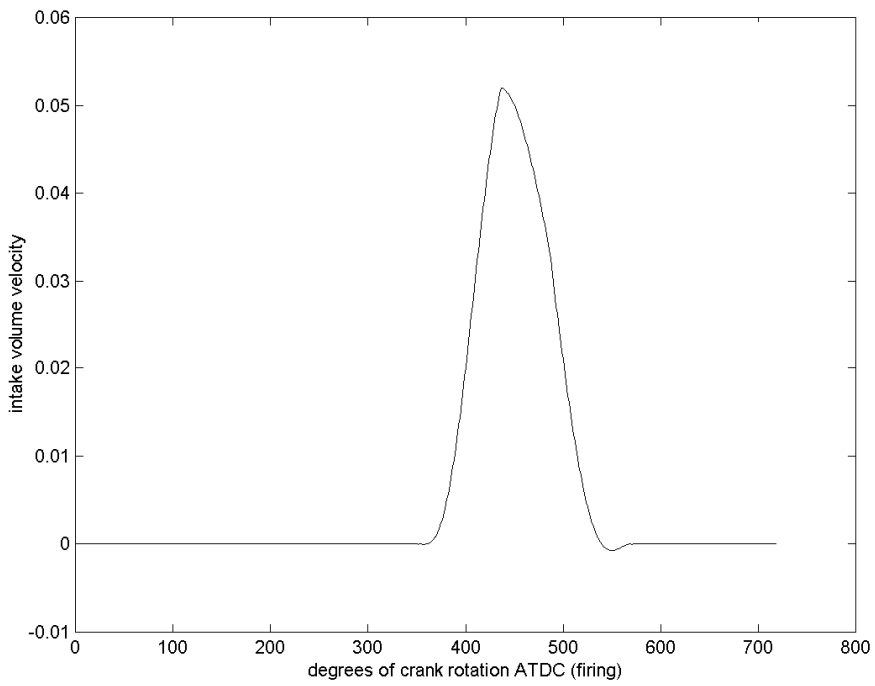


Figure: 10

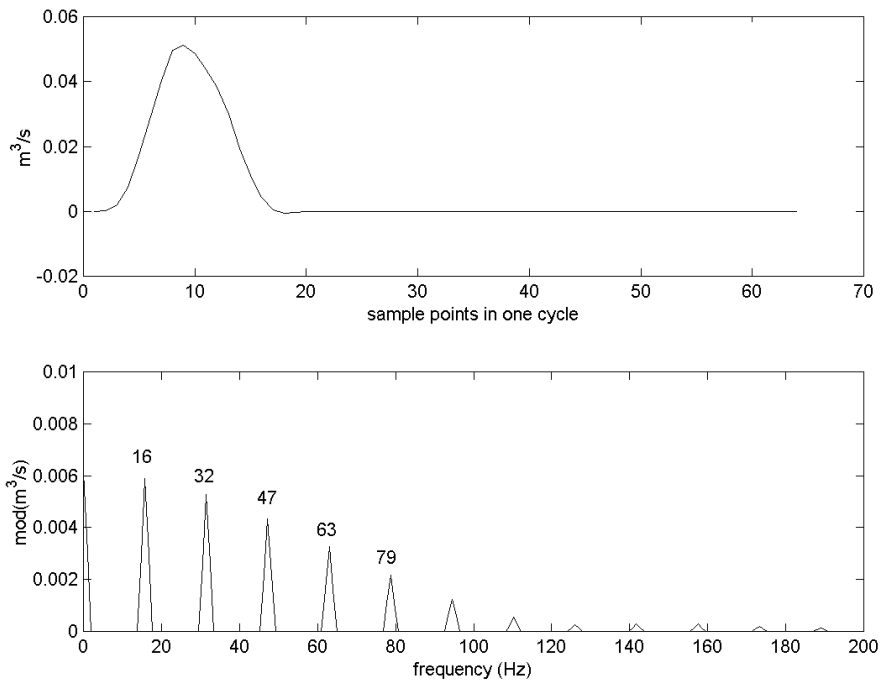


Figure: 11

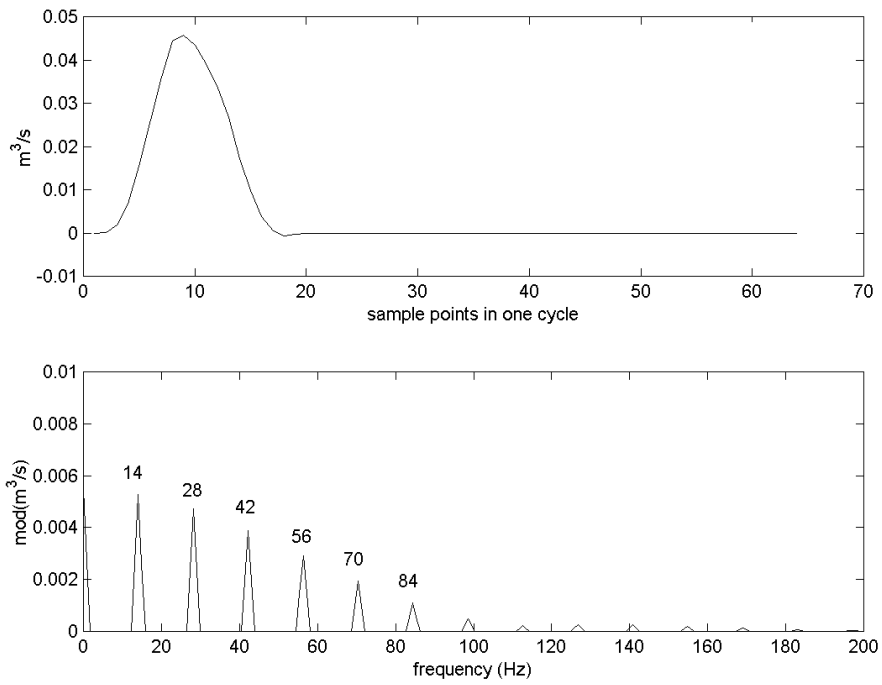


Figure: 12

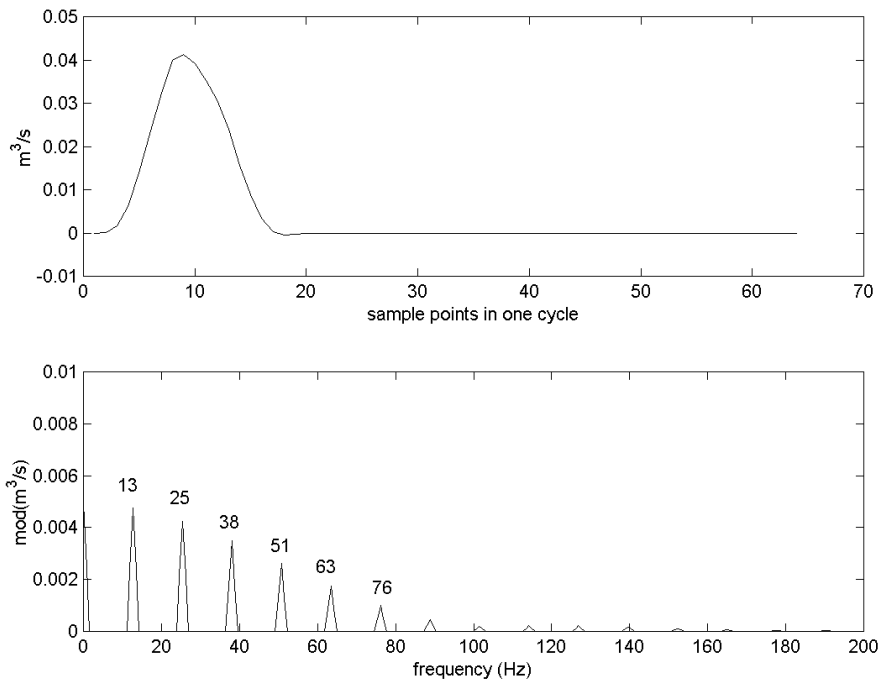


Figure: 13

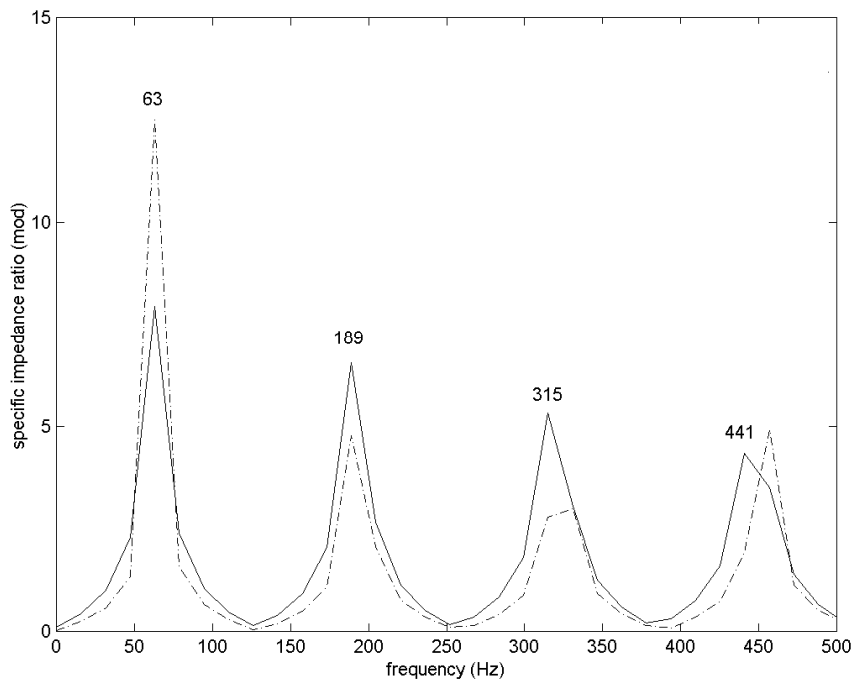


Figure: 14

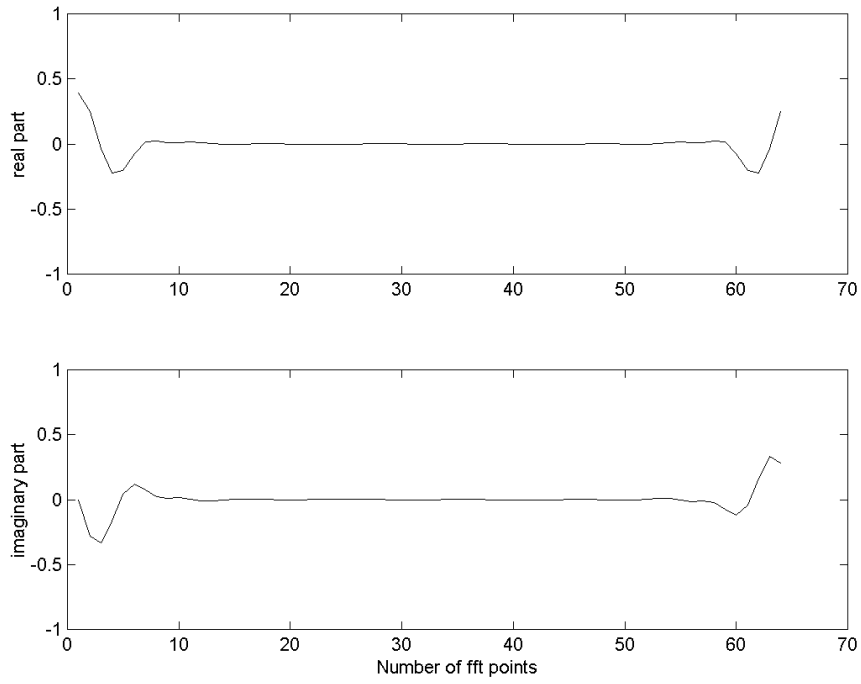


Figure: 15

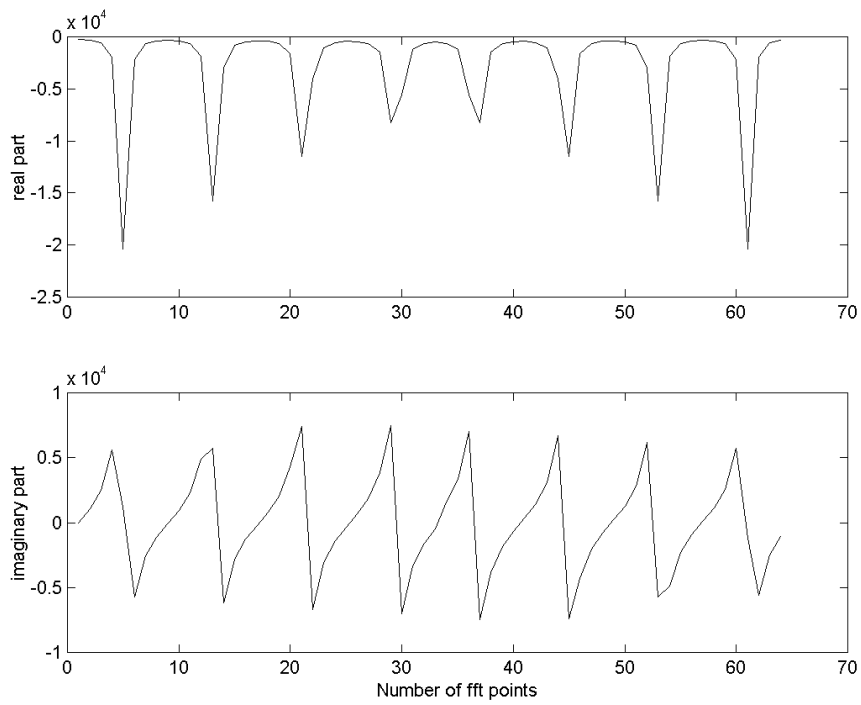


Figure: 16

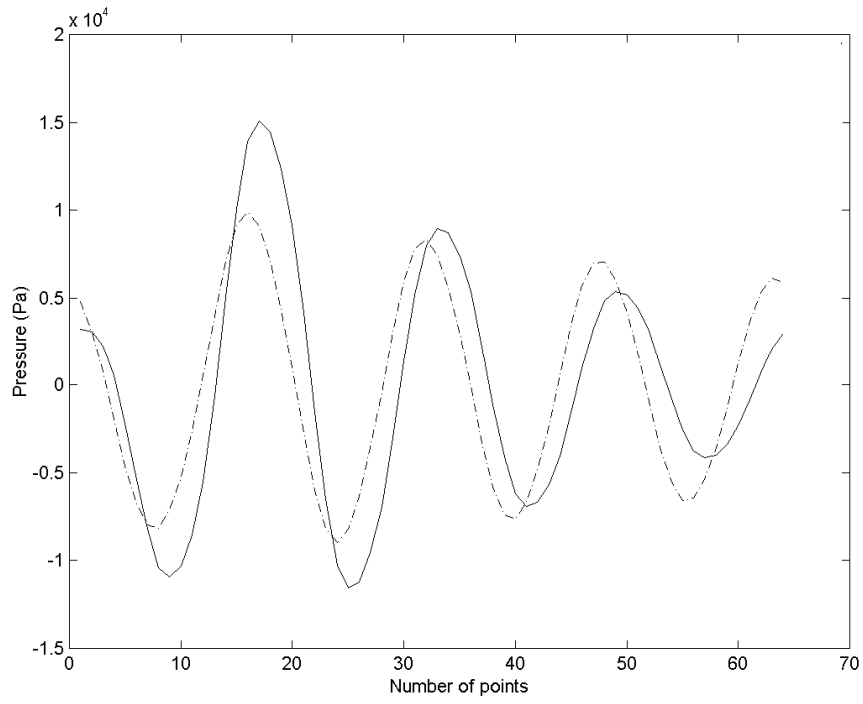


Figure: 17

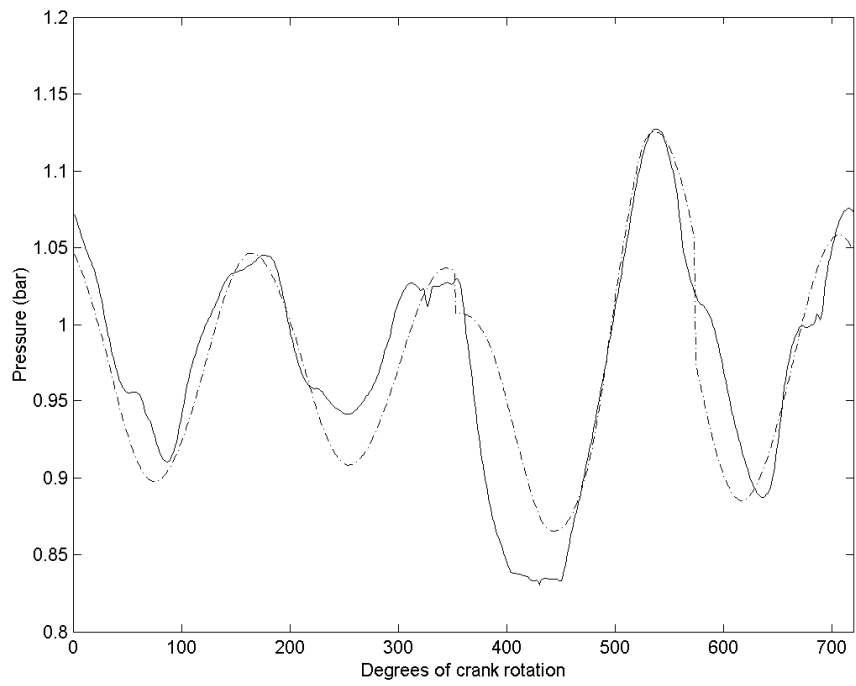


Figure: 18

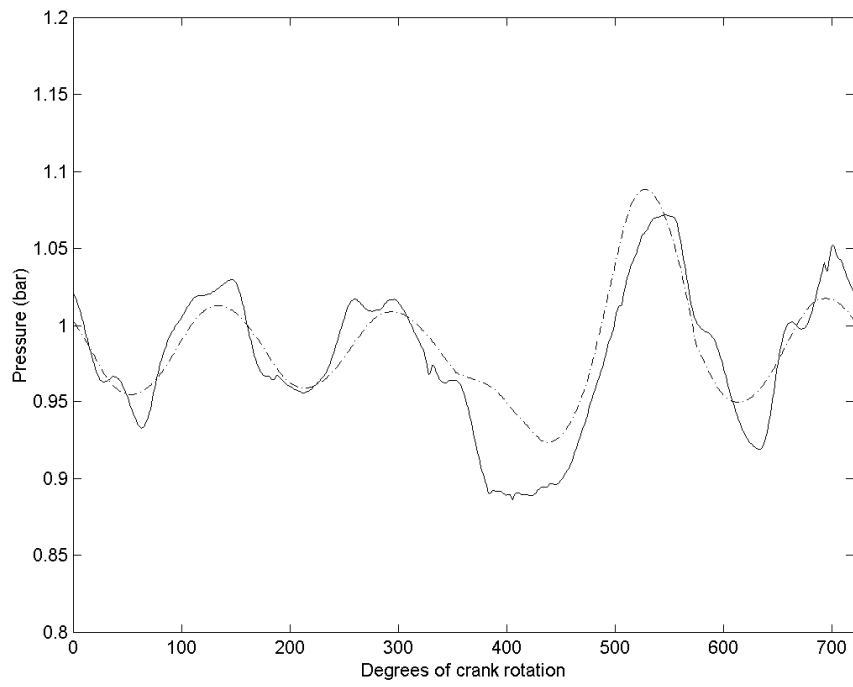


Figure: 19

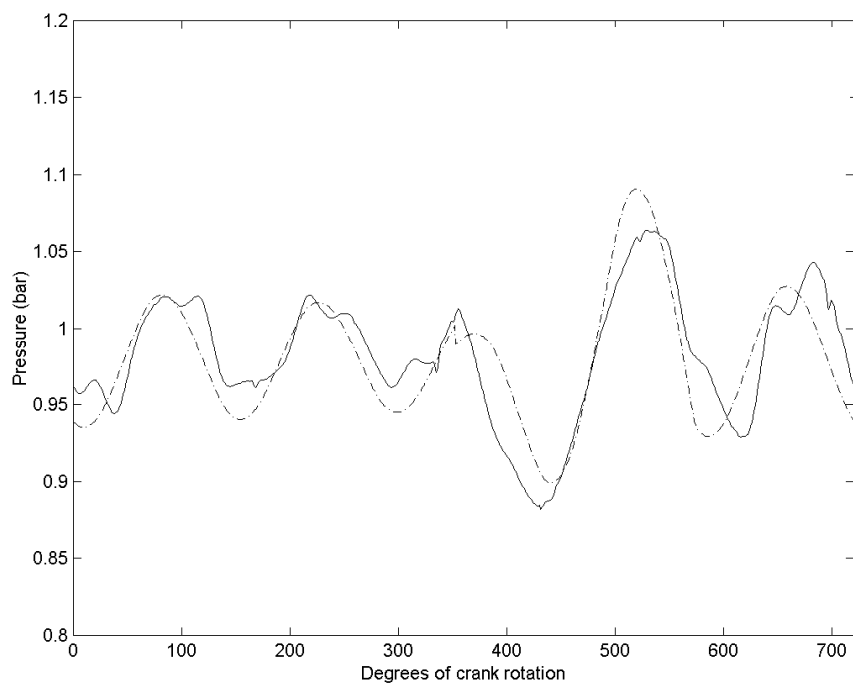


Figure: 20

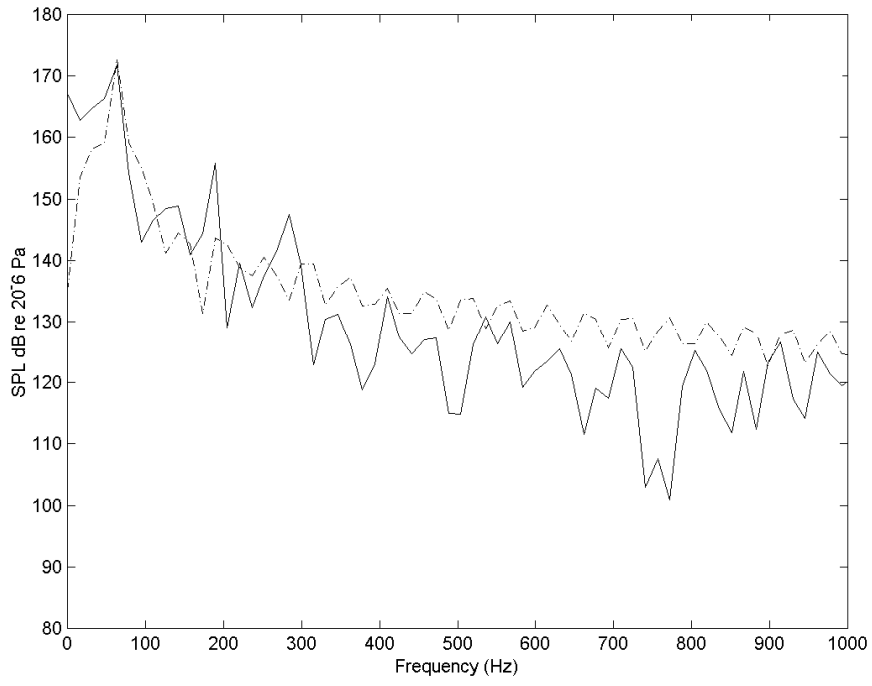


Figure: 21

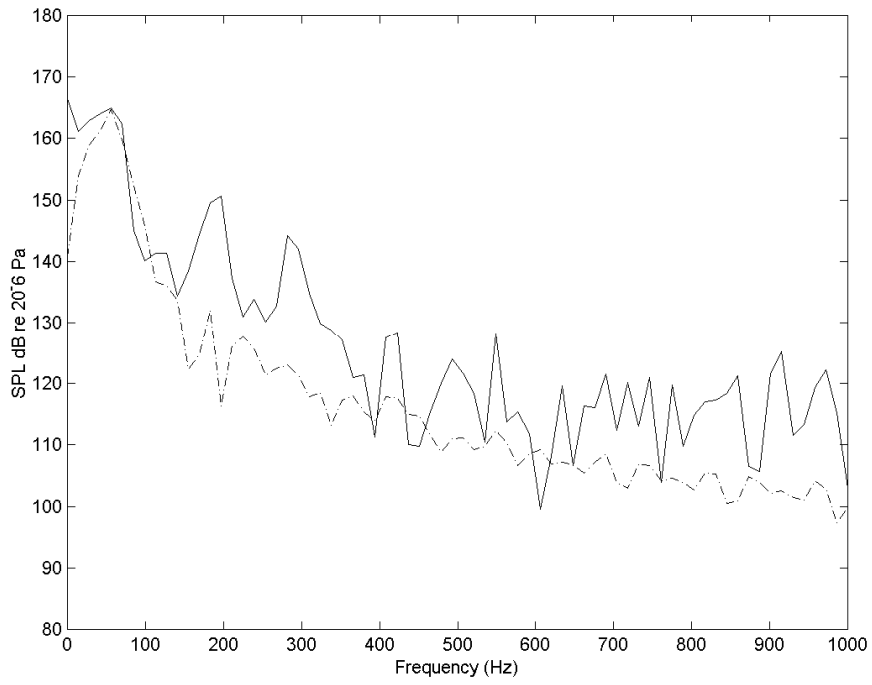


Figure: 22



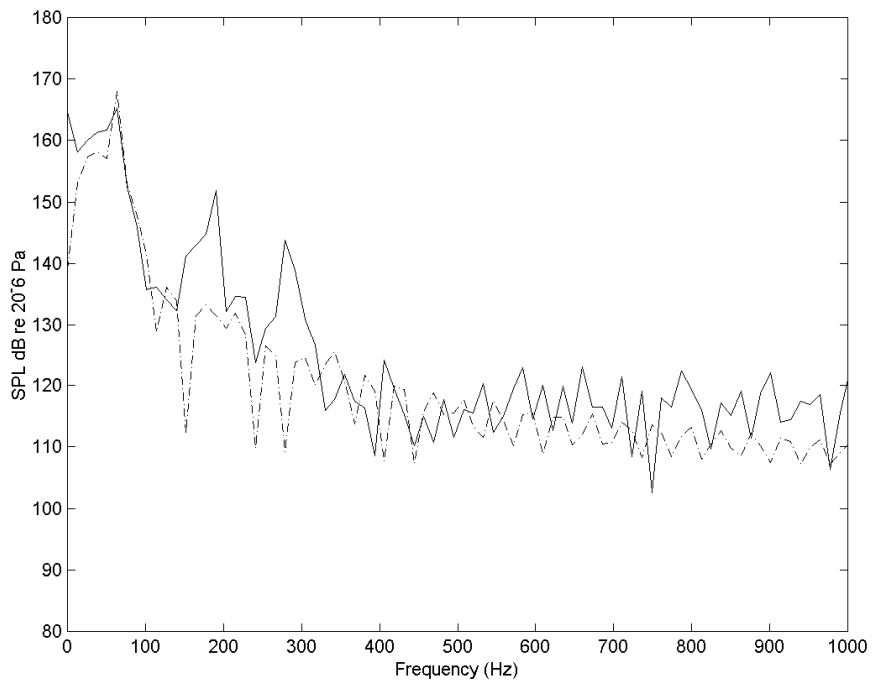


Figure: 23

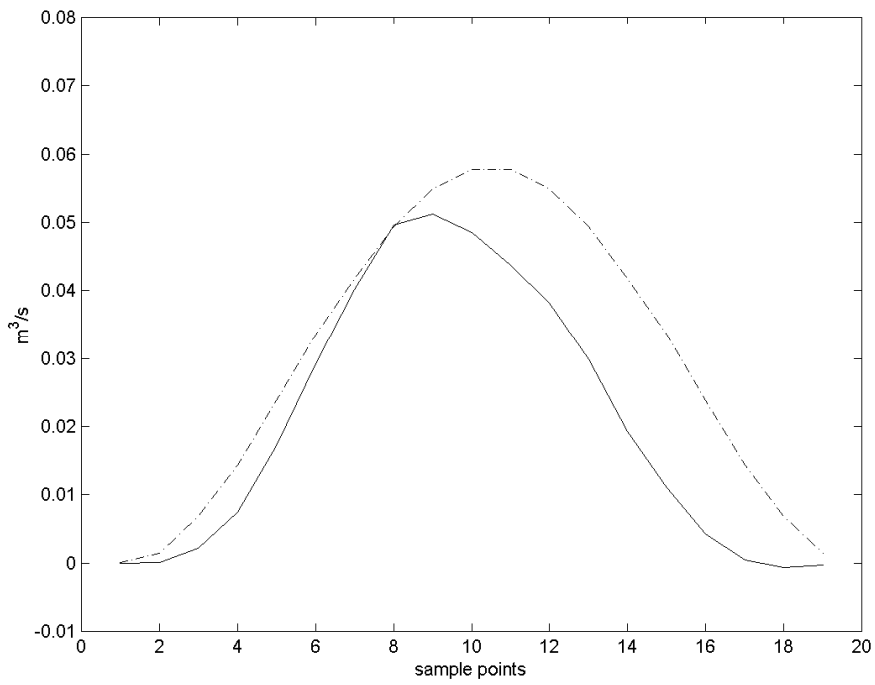


Figure: 24

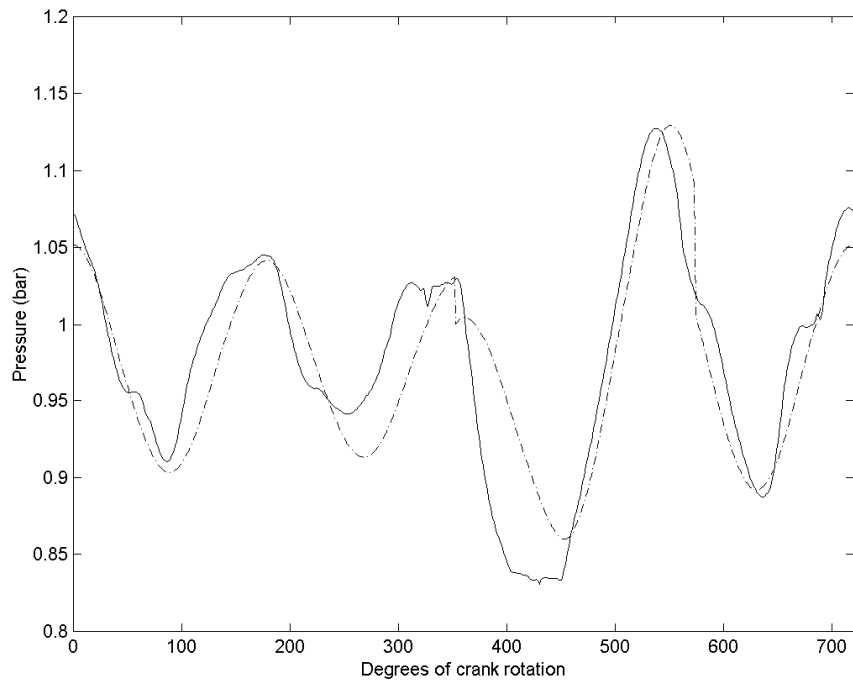


Figure: 25

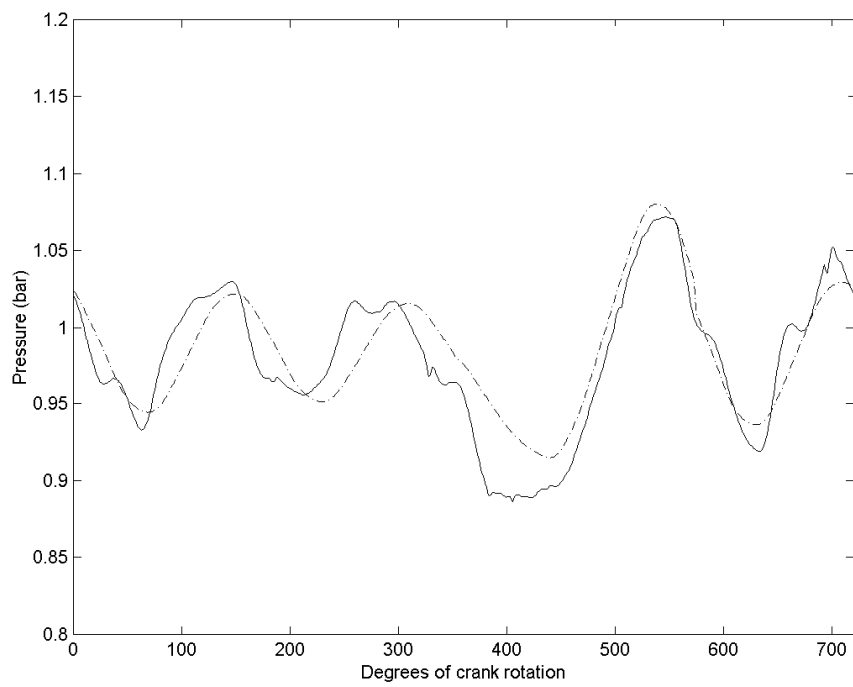


Figure: 26

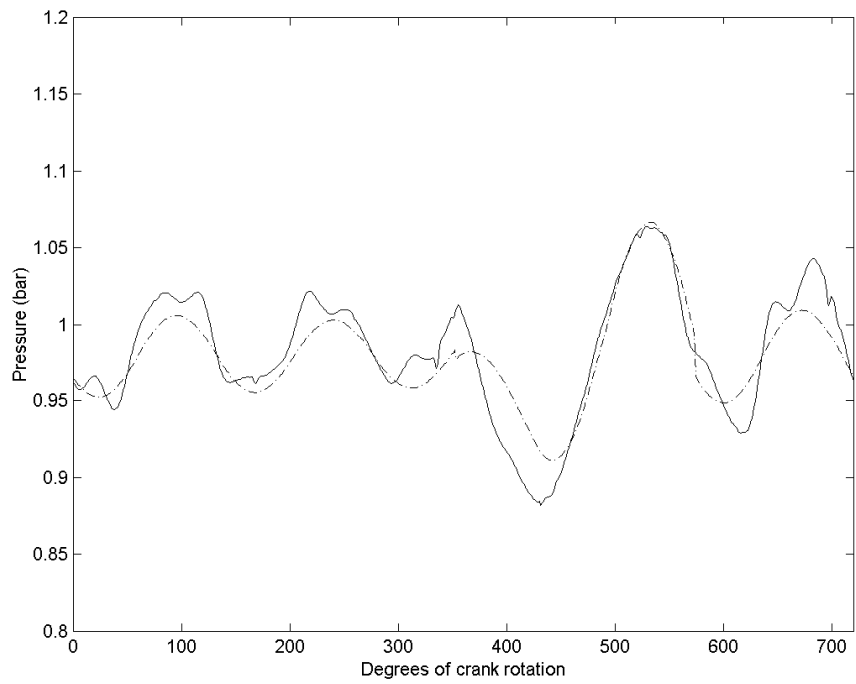


Figure: 27

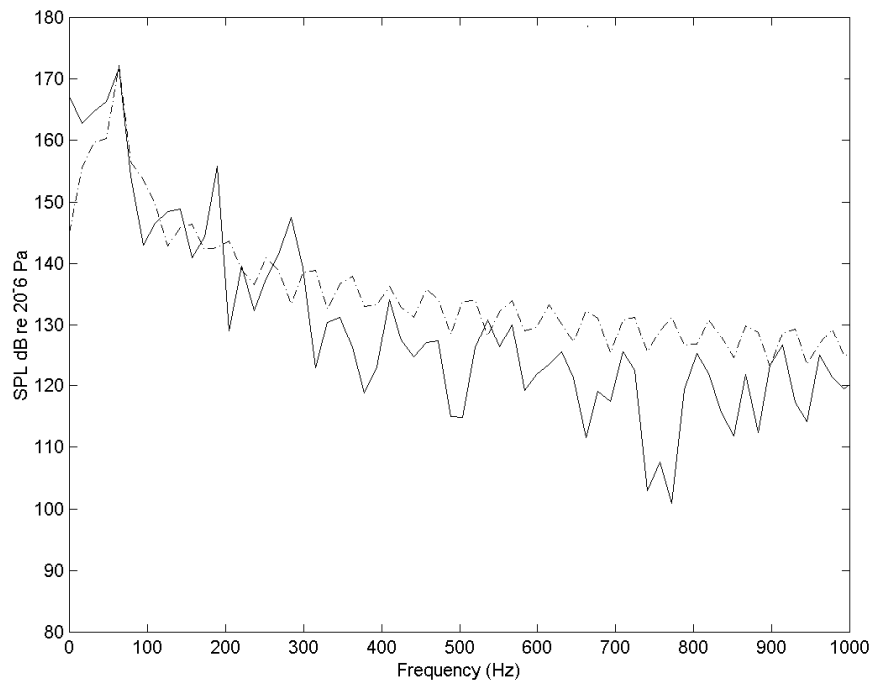


Figure: 28

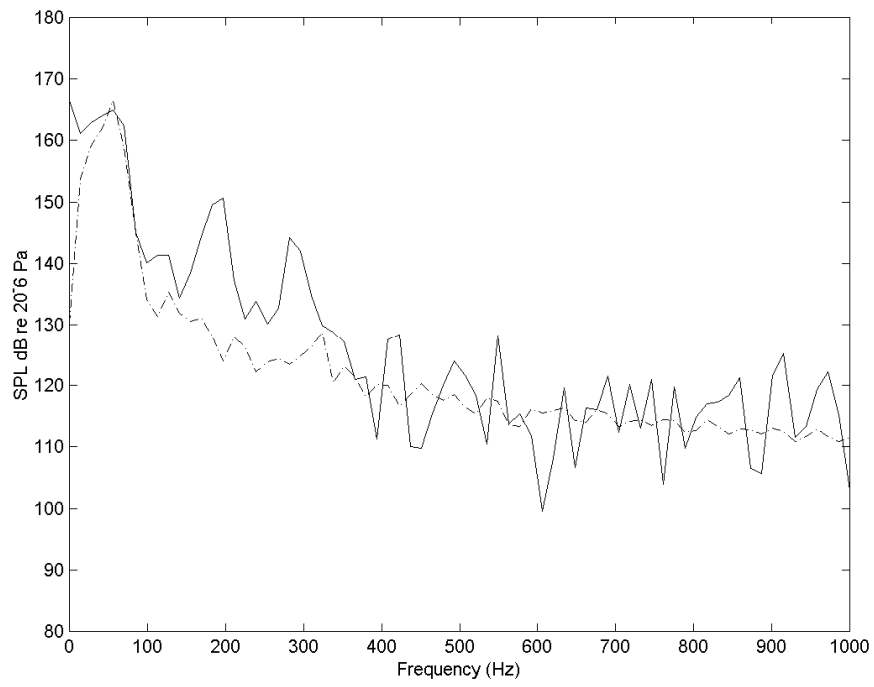


Figure: 29

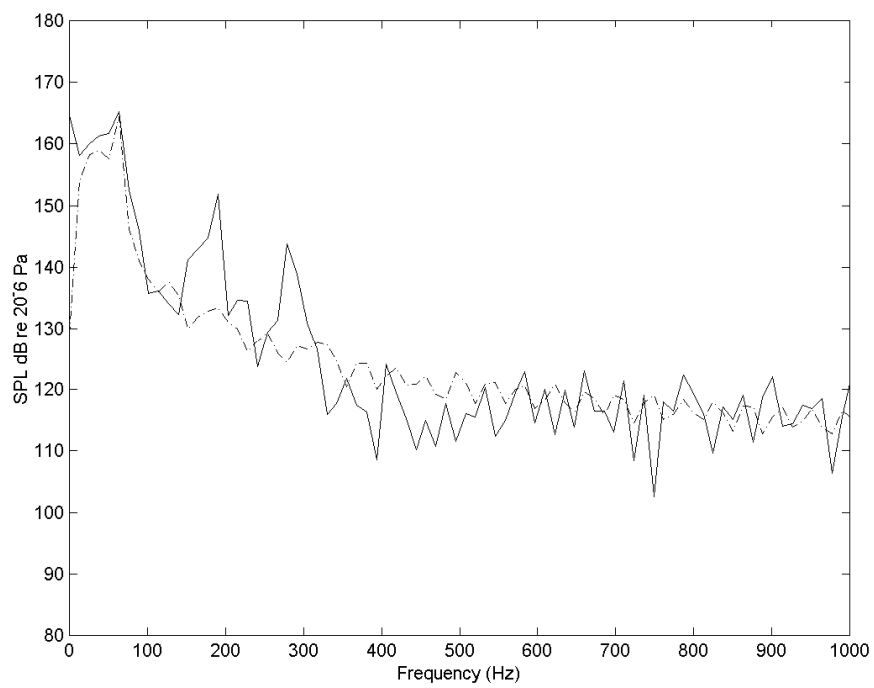


Figure: 30

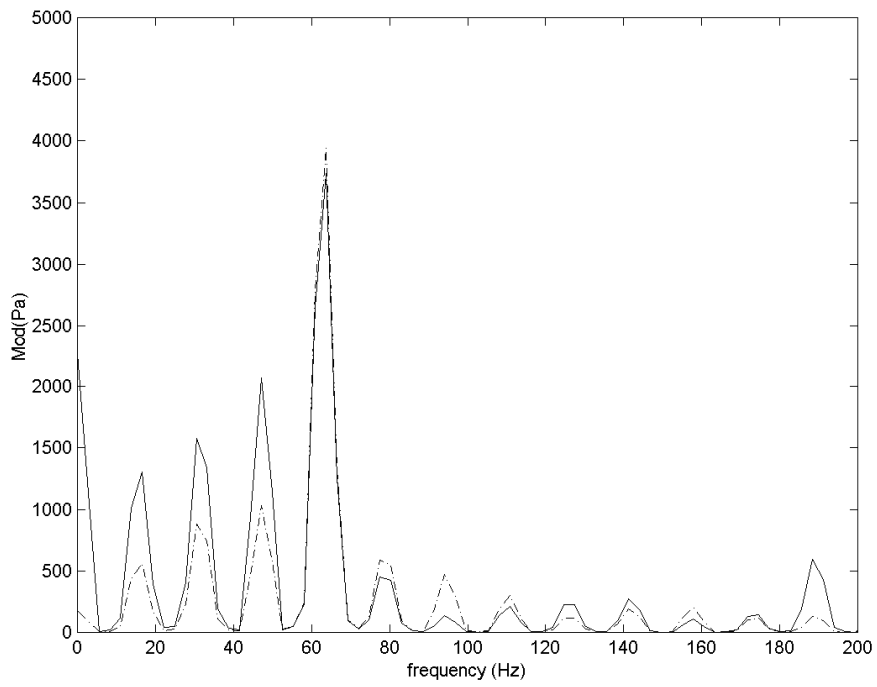


Figure: 31

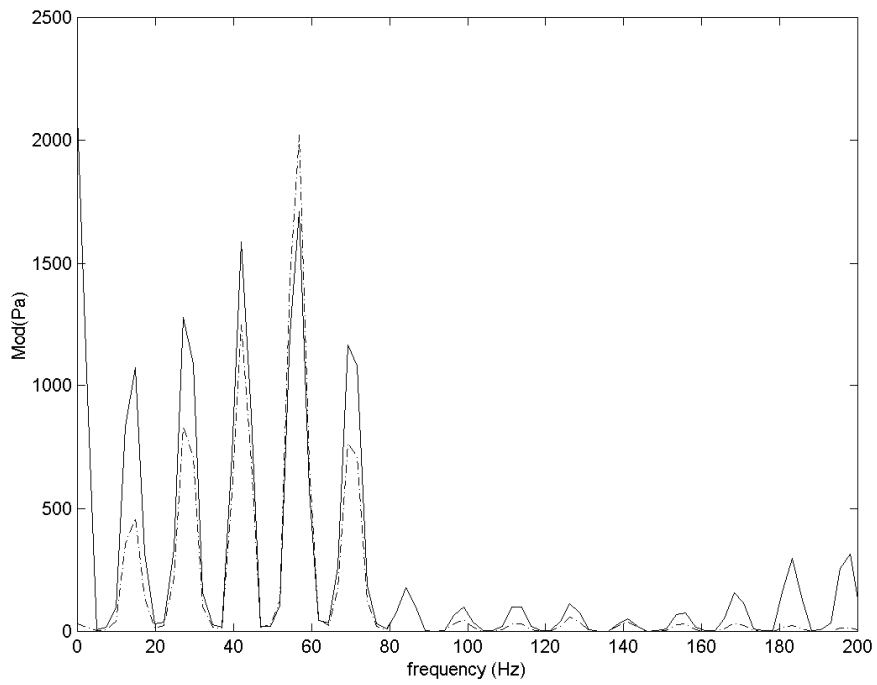


Figure: 32

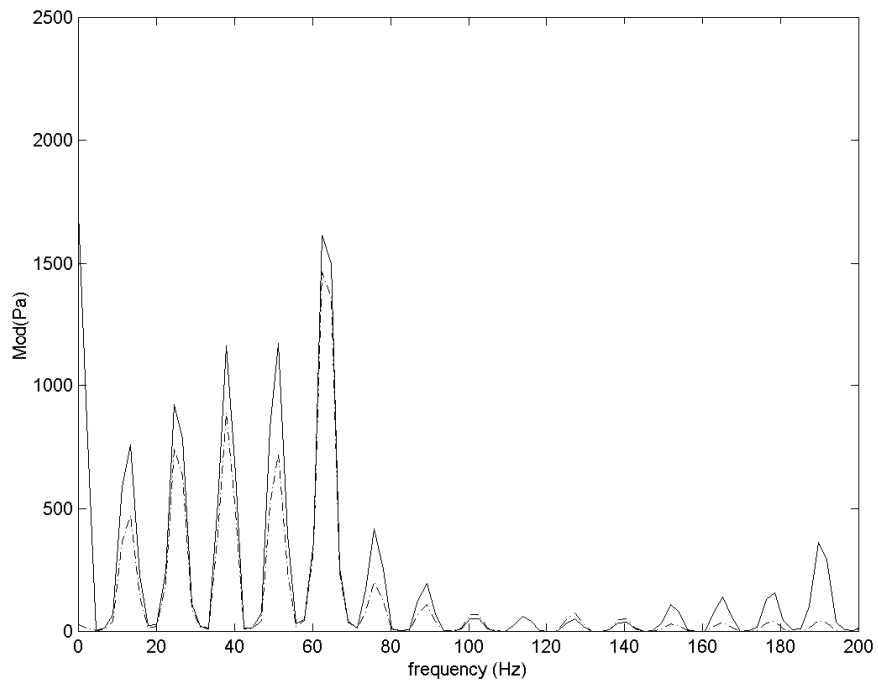


Figure: 33

ENDS.